Supplement of The Cryosphere, 13, 1709–1727, 2019
https://doi.org/10.5194/tc-13-1709-2019-supplement

The Cryosphere Open Access EGU

Supplement of

Multi-year evaluation of airborne geodetic surveys to estimate seasonal mass balance, Columbia and Rocky Mountains, Canada

Ben M. Pelto et al.

Correspondence to: Ben M. Pelto (pelto@unbc.ca)

Supplemental Information

Introduction

Here we provide additional details that relate to the data used in our study and associated methods.

S1. Snow Density

Given average winter snow depth >4 m on our study glaciers, we had numerous 6 m pits, and the time savings in conducting snow cores in lieu of snow pits allowed us to obtain more density measurements, more effectively reducing density uncertainty. The corer also allowed us to sample internal ice lenses, which are difficult to measure with a snow sampler. We used a snow saw (G3 bone saw) to collect discrete samples (3-25 cm length) from the snow cores (Gabrielli et al., 2010; McGrath et al., 2018), avoiding areas where the core broke, to ensure a known volume, with the goal of sampling nearly all intact material from the core (Figure S7). We noticed that core cuttings would accumulate at the bottom of the hole with each section of core taken, and so used care to avoid sampling these cuttings, which typically occupied the top 5-20 cm of the core but increased in amount with depth. We took spring snow density measurements at three locations at each site, (low, middle and high). Often, the density decreased with each subsequent core up-glacier, and thus we applied a linear regression of density and elevation to our depth measurements when converting to water equivalent. When there was no linear gradient, we averaged the snow density measurements to produce a glacier-wide snow density. We also found that if our lowest snow core was very low (e.g. on the toe of the glacier), these wind-swept locales often had the lowest density snow. In this case, we assigned the density of the lowest site to measurements of snow from the elevation range of the toe, and then used the upper two sites to determine density everywhere else, as to not bias the gradient or glacier-wide average with a sample unrepresentative of the glacier at-large.

S2. Uncertainty Assessment

We analyzed snow and ice-free terrain to derive statistical indicators of bias and data dispersion from ΔDEM over stable terrain using a late summer DEM as a reference, and report the mean, median and normalized median absolute deviation (NMAD) over stable terrain (Table 3). We bias correct the height change over the glacier surfaces using the systematic elevation difference over stable terrain (h_{dDEM}) in the ΔDEMs. This bias correction ranged from -0.09 to 0.05 m and averaged -0.01 m. NMAD reveals random errors that are typically below ±0.3 m, with a maximum of 0.6 m (Table 3). This maximum error occurred for Zillmer Glacier in late summer 2017 when the separation between site visit and ALS survey was large and new snow covered the glacier during the ALS survey (Table 2).

Random uncertainty stems from three sources that we assume to be independent: i) elevation change uncertainty ($\sigma h_{\Delta DEM}$), ii) glacier zone delineation uncertainty (σA), and iii) volume to mass density conversion uncertainty ($\sigma \rho$). Elevation change uncertainty is derived from the σ of height change over stable terrain (σh) after correction for effective sample size (N_{eff}):

$$\sigma h_{\Delta DEM} = \frac{2\sigma h}{\sqrt{N_{eff}}} \quad (1)$$

where the effective sample size is defined as (Bretherton et al., 1999):

$$N_{eff} = \frac{n \cdot dx}{2 \cdot L} \quad (2)$$

where *n* is the number of pixels of stable terrain, *dx* is the spatial resolution (1 m), and *L* is the decorrelation length. Stable terrain generally covered 10-20 km^2. We determined *L* by plotting semivariance (Figure S3) for randomly selected coordinate pairs (n=10,000) against distance for ten separate simulations and defined *L* as the distance at which semivariance becomes asymptotic (5% change threshold). Decorrelation length averaged 0.75 km and varied from 0.5 to 1.3 km. For delineation of ice/firn/snow zones from satellite imagery (Figure S1), we applied a buffering method (Granshaw and Fountain, 2006) to the perimeter of each zone that was not at the glacier boundary. Our satellite imagery resolution varied from 3 to 15 m, so we chose a buffer of four times the largest pixel size, to derive an uncertainty in area per zone:

$$\sigma A = perimeter \cdot \ 4 \cdot dx \quad (3)$$

This 60 m buffer accounts for uncertainty in zone delineation and changes in the positions of the zone boundaries occurring between ALS and satellite imagery acquisition dates. Due to the high resolution of our DEMs, planimetric uncertainties were all <1% of glacier area (average 0.6%), using a four-pixel buffer per Abermann et al. (2010), and they were omitted from uncertainty analysis (Belart et al., 2017). Total random uncertainty in volume change is:

$$\sigma \Delta V = \sqrt{(\sigma h_{\Delta DEM}(p + 5(1-p))A)^2 + \ (\sigma A \ \cdot \ h_{\Delta DEM})^2} \quad (4)$$

where A is the area of a given glacier and p is the percentage of surveyed area, which averaged 99.1% (Table 2). We assume a factor of five for the elevation change uncertainty of non-surveyed areas (Berthier et al., 2014). Random uncertainty on geodetic mass balance is:

$$\sigma \Delta M = \sum_i \sqrt{(\sigma \Delta V_i \ \cdot \rho_i)^2 \ + \ (\sigma \rho_i \cdot \Delta V)^2} \ \cdot \frac{A_i}{A_{tot}} \quad (5)$$

where ρ_i is individual density conversion values with associated uncertainties ($\pm \sigma \rho_i$) for spring snow, late summer snow, firn, and ice (Table 4). Prior to being summed to produce a final uncertainty, each zone (ice/firn/snow) is considered separately for B_a, with ΔV_i and A_i the volume and area change of each zone respectively.

Firn compaction or fresh snow on the surveyed surface introduce systematic uncertainty on geodetic balance. On Drangajökull ice cap, where B_w is more than 1 m w.e. greater than our average B_w, firn compaction and fresh snow densification increased geodetic B_w by 8%. Fresh snow off-glacier was negligible in all but a few cases. We thus assume a systematic uncertainty ($\sigma \Delta M_{sys}$) of 10% on $B_{a,w}$. Collectively, random and systematic uncertainty thus yield total uncertainty in mass balance:

$$\sigma B_{geod} = \sqrt{(\sigma \Delta M)^2 + \ (\sigma \Delta M_{sys})^2} \quad (6)$$

To determine uncertainty in glaciological mass balance, we derive a mean density (ρ) of mass change:

$$\rho = \frac{\rho_{ice} \cdot A_{ice} + \rho_{firn} \cdot A_{firn} + \rho_{snow} \cdot A_{snow}}{A_{tot}} \quad (7)$$

and uncertainty in height change:

$$\sigma\Delta h_{glac} = \sqrt{\sigma\Delta h_{surv}{}^2 + \sigma h_{obs}{}^2} \quad (8)$$

where $\sigma\Delta h_{surv}$ is the uncertainty in survey height correction applied to the glaciological balance, estimated as a 50% uncertainty in height correction (m). Survey uncertainty is assigned to glaciological balance (Table 3) instead of geodetic balance due to the near-synchronous timing of our ALS surveys and the staggered timing inherent in our glaciological data collection (Table 2). Locations where four measurements were taken indicated a σ of 4% for spring and 8% for summer, but we conservatively use 10% as the uncertainty in height change measurements to incorporate potential uncertainty introduced by small-scale variability of snow depth, probing of the incorrect surface, and possible self-drilling or plucking of ablation stakes (σh_{obs} of ± 0.20 m for B_a and ± 0.40 m for B_w). Uncertainty in glaciological mass balance is calculated as:

$$\sigma B_{a,w} = \sqrt{\sigma\Delta h_{glac}{}^2 \cdot \rho^2 + \sigma\rho^2 \cdot B_{a,w}{}^2} \quad (9)$$

where $\sigma\rho$ is the uncertainty on density taken to be 10% of ρ, to account for uncertainty in density measurements and extrapolation of those measurements. The uncertainty in extrapolation of glaciological observations to glacier-wide mass balance (σ_{Ext}) is taken as the σ of the different calculations of mass balance for each season. Glaciological mass balance uncertainty is thus:

$$\sigma B_{glac} = \sqrt{\sigma B_{a,w}{}^2 + \sigma_{Ext}{}^2} \quad (10)$$

For both geodetic and glaciological mass balance, B_s was derived as the difference of annual and summer balance (Eqn. 1), and thus uncertainty on B_s yields:

$$\sigma B_s = \sqrt{\sigma B_a{}^2 + \sigma B_w{}^2} \quad (11)$$

Table S1. Glacier-wide spring snow density from glaciological observations ($\rho_{spring.obs}$), and updated spring snow density using the linear relation ($\rho_{spring.lin}$) of Julian day versus snow density (Figure 3). No observed density implies no winter balance trip occurred, and no data in the $\rho_{spring.lin}$ column implies no B_{w_geod} was derived. When no spring glaciological visit occurred, the average spring snow density for the sites' available record was used.

Year	Glacier	$\rho_{spring.obs}$ (kg m^{-3})	$\rho_{spring.lin}$ (kg m^{-3})
2018	Zillmer	517	457
2018	Nordic	426	411
2018	Illecillewaet	—	461
2018	Haig	—	420
2018	Conrad	407	413
2018	Kokanee	395	419
2017	Zillmer	381	492
2017	Nordic	403	463

2017	Illecillewaet	443	449
2017	Haig	420	420
2017	Conrad	500	518
2017	Kokanee	415	517
2016	Zillmer	447	459
2016	Nordic	541	496
2016	Illecillewaet	456	456
2016	Haig	420	420
2016	Conrad	480	453
2016	Kokanee	459	459
2015	Zillmer	554	—
2015	Nordic	452	416
2015	Illecillewaet	—	—
2015	Haig	420	—
2015	Conrad	481	472
2015	Kokanee	466	—

Table S2. Shallow firn core densities. Presumed year is the year the firn was deposited. Kokanee 2016 sample presumed age 2013 was directly overlain by 2016 snow (Figure S8); mass balance observations in 2015 indicated no retained snow in 2015, and a loss of 2014 snow at the core location.

Glacier	Obs. Year	Presumed Year	Depth (cm)	Firn length (cm)	Elev. (m)	Density (kg m^{-3})	Years back
Nordic	2017	2016	610-960	350	2745	584	1
Nordic	2017	2015	960-1020	60	2745	669	2
Nordic	2017	2014	1020-1100	80	2745	664	3
Zillmer	2015	2014	455-585	130	2527	623	1
Zillmer	2017	2016	510-555	55	2527	553	1
Kokanee	2016	2013	420-440	20	2660	776	3
Kokanee	2017	2016	540-605	65	2660	650	1
Illecillewaet	2017	2016	500-335	165	2606	685	1

Table S3. Height change uncertainty as defined in supplemental equations 1 and 2.

Year	Glacier	$\sigma h_{\Delta DEM}$ B_a (m)	$\sigma h_{\Delta DEM}$ B_w (m)
2018	Zillmer	—	0.04
2018	Nordic	—	0.05
2018	Illecillewaet	—	0.07
2018	Haig	—	0.09
2018	Conrad	—	0.05

2018	Kokanee	—	0.07
2017	Zillmer	0.03	0.05
2017	Nordic	0.02	0.02
2017	Illecillewaet	0.03	0.07
2017	Haig	0.05	0.07
2017	Conrad	0.02	0.05
2017	Kokanee	0.02	0.07
2016	Zillmer	0.02	0.06
2016	Nordic	0.03	0.06
2016	Illecillewaet	0.05	0.08
2016	Haig	0.04	0.07
2016	Conrad	0.02	0.06
2016	Kokanee	0.02	0.07
2015	Zillmer	—	—
2015	Nordic	0.03	0.02
2015	Illecillewaet	—	—
2015	Haig	—	—
2015	Conrad	0.02	0.04
2015	Kokanee	—	—
All	Average	0.03	0.06

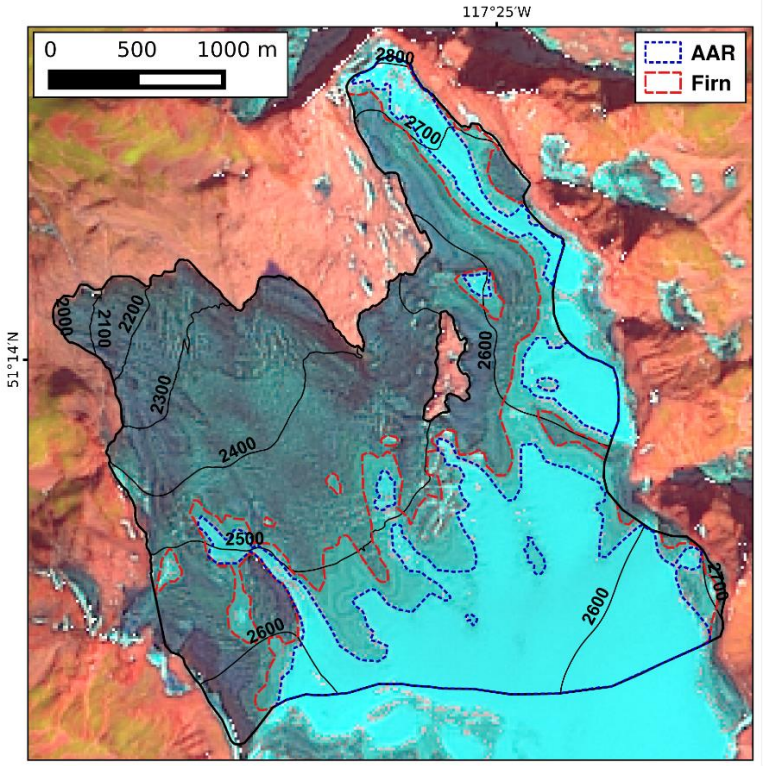

Figure S1: Surface classification of the Illecillewaet Glacier with a pan-sharpened Landsat 8 image from August 12, 2015. Firn area, and accumulation area are shown, with the remainder of the glacier (black outline), classified as ice.

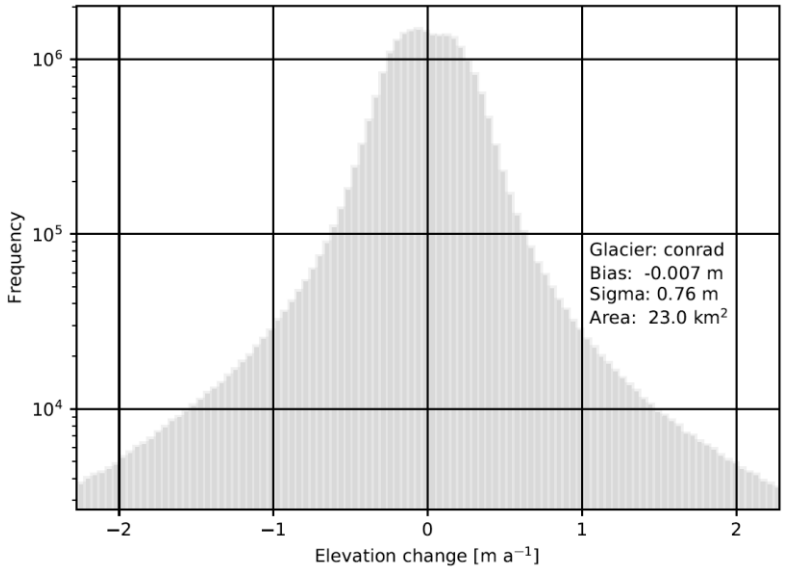

Figure S2: Example plot of off-ice observations for Conrad Glacier. Elevation change is plotted as off-ice observations between the late summer 2016 and late summer 2017 DEMs for Conrad Glacier. Height change was bias corrected by -0.007 m based upon these observations. Off-ice area used in this plot covered 23 km^2.

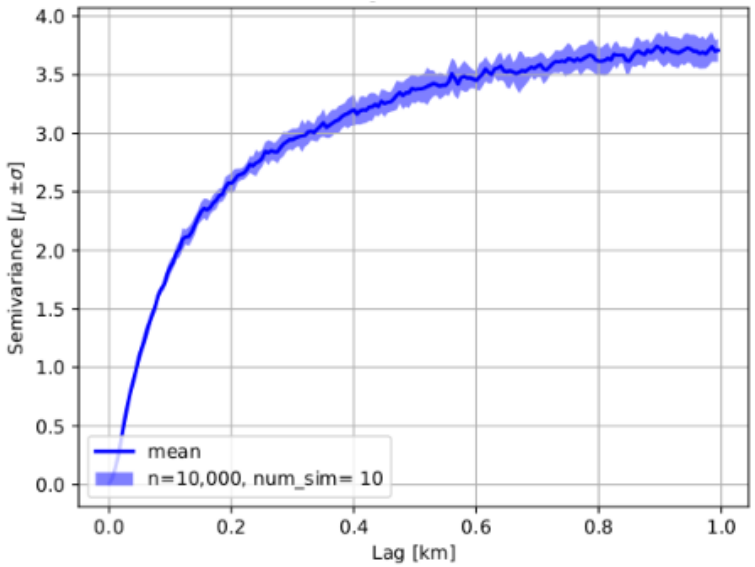

Figure S3: Example semivariogram for Conrad Glacier, winter 2018. The variogram was constructed using 10,000 random samples over 10 simulations. Decorrelation length was defined as the distance at which semivariance becomes asymptotic (5% change threshold), 900 m in this example.

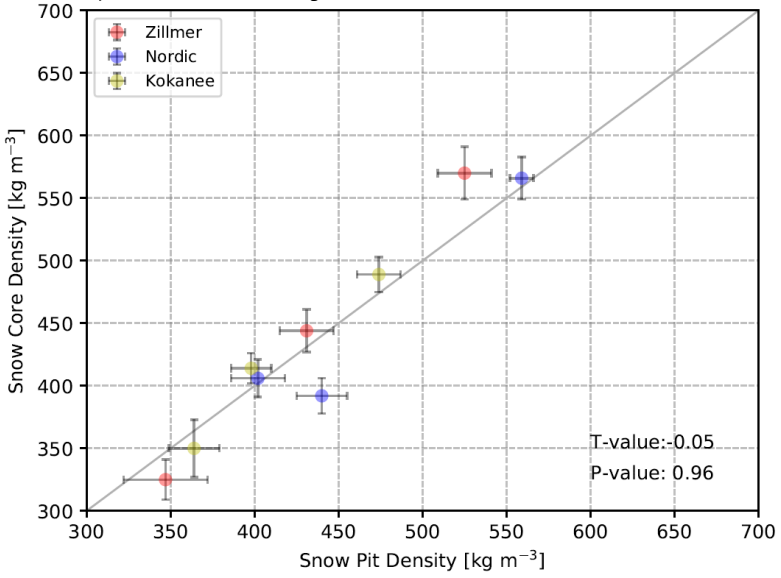

Figure S4: Comparison of snow pits and snow cores taken side-by-side. We conducted nine side-by-side pit/core comparisons which showed that our pit densities were a 0.2 ± 5.7% heavier. The average absolute magnitude of disagreement between pit and core density was 4.8% ranging from -11.5% to +8%. For snow pits we took a 100 cm^{-3} sample every 10 centimeters depth down the snow pit wall. For snow cores, we used a snow saw to take samples from each core, of up to 25 cm-length. Taking discrete samples allowed for samples of known volume, avoiding broken sections of core, and avoided measuring the core fillings which fall to the bottom of the hole upon removal of the barrel after taking each core (~1 m-length), then becoming the top of the subsequent core.

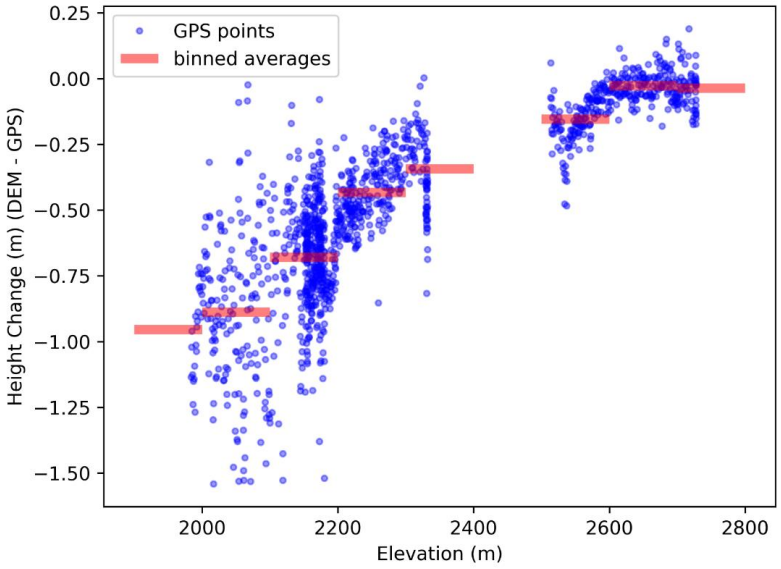

Figure S5: Zillmer Glacier kinematic GPS survey points subtracted from the subsequent ALS survey. The survey points were collected on August 12, 14 and 16, 2016 while the ALS survey was conducted on September 14, 2016. Height change points are averaged over 100 m elevation bands, and then assigned a density based upon surface classification from satellite observations to convert height change to water equivalent. Glaciological data are then corrected with this data. Data between 2300-2500 m not shown as the base-station unit failed during this portion of surveying. Typically, time between GPS surveys and LiDAR acquisition was between 0-21 days.

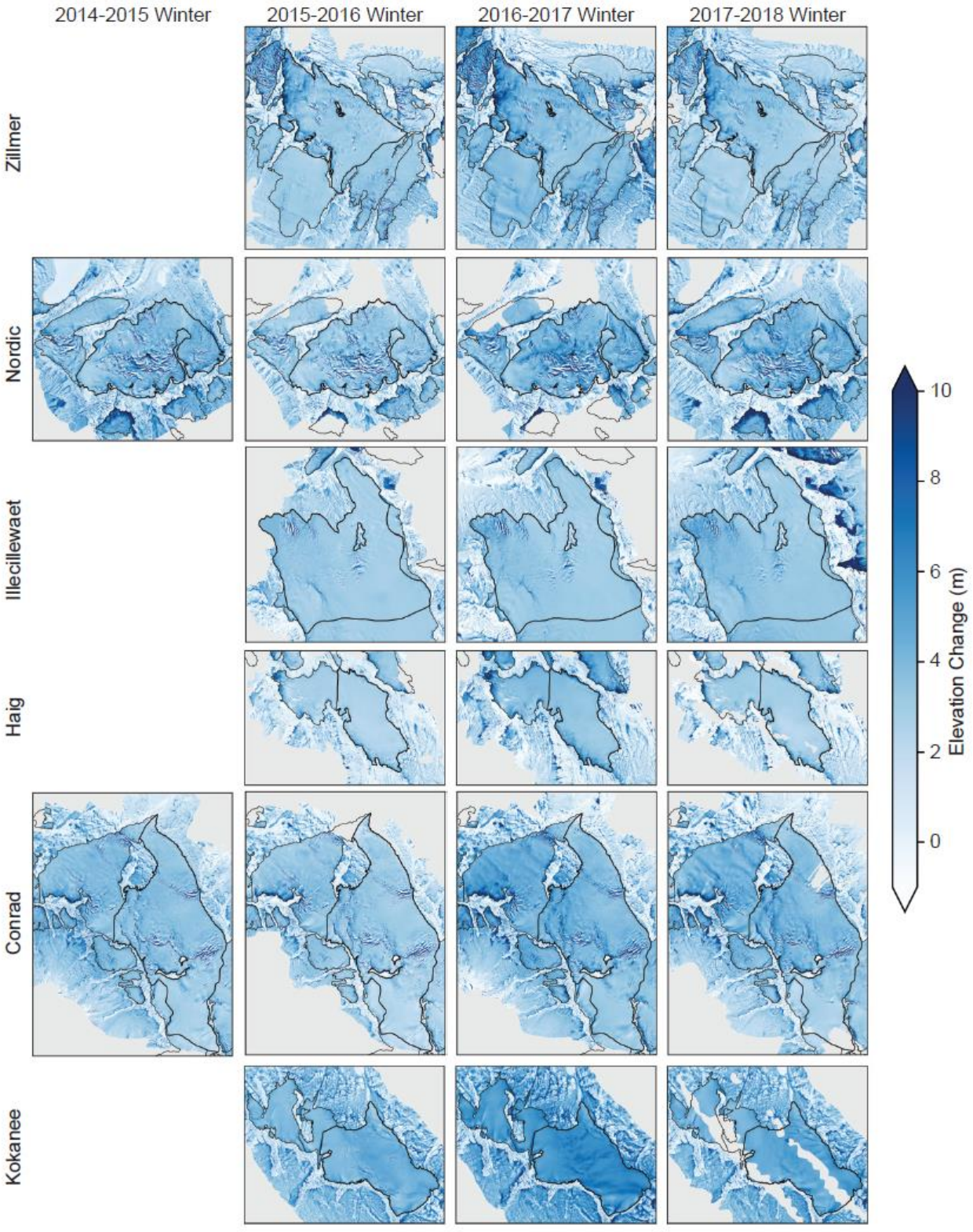
2014-2015 Winter
2015-2016 Winter
2016-2017 Winter
2017-2018 Winter
Zillmer
Nordic
Illecillewaet
Haig
Conrad
Kokanee
Elevation Change (m)
0
2
4
6
8
10

Figure S6: Winter surface height change for the Zillmer, Nordic, Illecillewaet, Haig, Conrad, and Kokanee glaciers for between 2014 and 2018. Study glaciers are outlined with thick black line and other glaciers with a thin black line.

Figure S7. Sampling a snow core on the Kokanee glacier. Snow saw used to cut samples from the core. Photo by Jill Pelto.

Figure S8. Snow and firn core from Kokanee Glacier, April 19, 2016. Core at photo bottom is snow, lower finger pointing to the snow-firn transition, and upper finger pointing to a dirty horizon marking an annual layer in the firn. Photo by Jill Pelto.